Molecular Pharmacology Fast Forward. Published on July 16, 2018 as DOI: 10.1124/mol.118.112375
This article has not been copyedited and formatted. The final version may differ from this version.

MOL #112375

The conoRFamide RPRFa stabilizes the open conformation of Acid-Sensing Ion Channel 3 via the nonproton ligand sensing domain

Melissa Reiners, Michael A. Margreiter, Adrienne Oslender-Bujotzek, Giulia Rossetti, Stefan Gründer, and Axel Schmidt

Institute of Physiology, RWTH Aachen University, Pauwelsstrasse 30, D-52074 Aachen, Germany (M.R., A.O.-B., S.G., A.S.); and Department of Oncology, Hematology and Stem Cell Transplantation, RWTH Aachen University, Pauwelsstraße 30, D-52074 Aachen, Germany (G.R.); and Computational Biomedicine – Institute for Advanced Simulation (IAS)/Institute of Neuroscience and Medicine (INM) and Jülich Supercomputing Centre (JSC), Forschungszentrum Jülich, D-52425 Jülich, Germany (M.A.M., G.R.)

Molecular Pharmacology Fast Forward. Published on July 16, 2018 as DOI: 10.1124/mol.118.112375
This article has not been copyedited and formatted. The final version may differ from this version.

Running title: RPRFa stabilizes the open conformation of ASIC3

Address correspondence to: Axel Schmidt or Stefan Gründer, Institute of Physiology, RWTH Aachen University, Pauwelsstrasse 30, D-52074 Aachen, Germany, Tel.: +49 241-80-88800; Fax: +49 241-80-82434; E-mail: axel.schmidt1@rwth-aachen.de; sgruender@ukaachen.de

This manuscript contains

33 text pages,

7 figures,

44 references,

223 words in the Abstract,

746 words in the Introduction, and

1,251 words in the Discussion

ABBREVIATIONS: ASIC, acid-sensing ion channel; azF, 4-Azido-L-phenylalanine; DEG/ENaC, degenerin/epithelial Na^+ channel; ECD, extracellular domain; FaNaC, FMRFamide-activated Na^+ channel; GMQ, 2-guanidine-4-methylquinazoline; HyNaC, Hydra Na^+ channel; NPLSD, nonproton ligand sensing domain; TMD, transmembrane domain; wt, wild type.

Molecular Pharmacology Fast Forward. Published on July 16, 2018 as DOI: 10.1124/mol.118.112375
This article has not been copyedited and formatted. The final version may differ from this version.

ABSTRACT

Acid-sensing ion channel 3 (ASIC3) is a proton-gated Na^+ channel with important roles in pain. ASIC3 quickly desensitizes within less than a second, limiting its capacity to sense sustained acidosis during pain. RFamide neuropeptides are modulators of ASIC3 that slow its desensitization and induce a variable sustained current. The molecular mechanism of slowed desensitization and the RFamide binding site on ASIC3 are unknown. RPRFamide, a RFamide from the venom of a cone snail, has a comparatively high affinity for ASIC3 and strongly slows its desensitization. Here we show that covalent binding of a UV-sensitive RPRFamide variant to ASIC3 prevents desensitization, suggesting that RPRFamide has to unbind from ASIC3 before it can desensitize. Moreover, we show by in silico docking to a homology model of ASIC3 that a cavity in the lower palm domain, which is also known as the nonproton ligand sensing domain, is a potential binding site of RPRFamide. Finally, using extensive mutagenesis of residues lining the nonproton ligand sensing domain, we confirm that this domain is essential for RPRFamide modulation of ASIC3. As comparative analysis of ASIC crystal structures in the open and the desensitized conformation suggests that the lower palm domain contracts during desensitization, our results collectively suggest that RPRFamide, and probably also other RFamide neuropeptides, bind to the nonproton ligand sensing domain to stabilize the open conformation of ASIC3.

Molecular Pharmacology Fast Forward. Published on July 16, 2018 as DOI: 10.1124/mol.118.112375
This article has not been copyedited and formatted. The final version may differ from this version.

Introduction

Acid-sensing ion channels (ASICs) are Na^+ channels gated by extracellular protons. They assemble as trimers (Bartoi et al., 2014). Each subunit has a topology with two transmembrane domains (TMDs) and a large extracellular domain (ECD), which is composed of 7 α helices and 12 β strands that fold into a structure that has been compared with a clenched hand (Jasti et al., 2007). In this picture, the two TMDs build the forearm and the ECD is composed of a palm domain, a finger, a knuckle, and a thumb domain that surround the central β-ball domain. A pocket in the ECD containing several conserved acidic residues has been implicated in binding protons (Jasti et al., 2007) and gating modifier toxins (Baconguis and Gouaux, 2012; Dawson et al., 2012).

ASIC3 is an isoform that is predominantly expressed in the peripheral nervous system, where it contributes to the detection of painful acidosis (Deval and Lingueglia, 2015; Sluka and Gregory, 2015). It is expressed in primary muscle afferents and mediates muscle pain in ischemic-like conditions (Molliver et al., 2005; Ross et al., 2016; Sluka et al., 2003), for example during muscle fatigue. Muscle incision also decreases pH and ASIC3 also mediates post-incisional (post-operative) pain (Deval et al., 2011). Its expression is particularly high in afferents innervating the heart muscle, where it probably mediates the pain during myocardial ischemia (angina) (Benson et al., 1999; Sutherland et al., 2001). Moreover, in rodents it contributes to cutaneous acid pain (Deval et al., 2008), to hyperalgesia associated with neuropathic pain (Omori et al., 2008), to acute arthritic pain (Ikeuchi et al., 2009) and to itch sensation in response to acid and pruritogens (Peng et al., 2015). Thus, ASIC3 has a well-established role in the detection of pain associated with sustained acidosis. In addition, ASIC3 is expressed in cell models of glioblastoma (Tian et al., 2017) where it might sense the sustained acidic microenvironment of a brain tumor.

Upon rapid application of protons, however, ASIC3 completely desensitizes with a time constant of 0.3 sec (Sutherland et al., 2001). During a slight but prolonged acidosis, it

Molecular Pharmacology Fast Forward. Published on July 16, 2018 as DOI: 10.1124/mol.118.112375
This article has not been copyedited and formatted. The final version may differ from this version.

desensitizes without apparent opening (Gründer and Pusch, 2015), clearly limiting its capacity to sense sustained acidosis. Although it has been shown that the overlap of steady-state desensitization and activation curves of ASIC3 leads to a small window current in a tiny window of pH values that roughly correspond to the pH values reached during myocardial ischemia (Yagi et al., 2006), it is likely that different modulators interact with ASIC3 to either extend the window current (Deval et al., 2008; Marra et al., 2016) or to induce sustained currents.

One group of such modulators are RFamide neuropeptides (Vick and Askwith, 2015). The prototypical RFamide is FMRFamide, an important neurotransmitter in different invertebrates. The main effect of FMRFamide is a slowing of desensitization (prolonging opening) of ASICs. In addition, it induces a variable sustained current (Askwith et al., 2000). Mammalian RFamides, neuropeptide FF (FLFQPQRFamide) and neuropeptide AF (AGEGLNSQFWSLAAPQRFamide), have similar effects, which are smaller, however (Askwith et al., 2000). Although RFamides bind to the open conformation of ASICs (Chen et al., 2006b), the on-rate to their binding site is relatively slow and therefore, binding to the closed conformation is usually necessary for an efficient modulation (Askwith et al., 2000; Chen et al., 2006b). Neither the mechanism by which RFamides slow desensitization and induce a sustained current nor their binding site on ASICs are known.

Recently, RPRFamide (RPRFa), a cono-RFamide that has a comparatively high affinity to ASIC3 and strongly slows its desensitization, has been isolated from the venom of the cone snail *Conus textile* (Reimers et al., 2017). RPRFa increases the excitability of sensory neurons expressing ASIC3 and injection of RPRFa into the gastrocnemius muscle of mice enhances muscle pain in response to acidic stimuli (Reimers et al., 2017). Thus, RPRFa is an ideal tool to study the modulation of ASIC3 by RFamides. Here, we reveal that RPRFa has to unbind from ASIC3 before the channel can desensitize, explaining the slowed desensitization. Moreover, we show that a cavity in the lower ECD of ASIC3, which is surrounded by the base

Molecular Pharmacology Fast Forward. Published on July 16, 2018 as DOI: 10.1124/mol.118.112375
This article has not been copyedited and formatted. The final version may differ from this version.

of the three palm domains, the so-called nonproton ligand sensing domain (NPLSD), is important for the modulation by RPRFa. Since the lower palm domain contracts during desensitization (Baconguis et al., 2014; Baconguis and Gouaux, 2012), our results provide a mechanistic explanation for the functional effects of RFamides on ASIC3 and strongly suggest that the NPLSD is the RFamide binding site on ASIC3.

Molecular Pharmacology Fast Forward. Published on July 16, 2018 as DOI: 10.1124/mol.118.112375
This article has not been copyedited and formatted. The final version may differ from this version.

Materials and Methods

Peptides and Chemicals. RPRFa and RPR[azF]a were synthesized by ProteoGenix (Schiltigheim, France) with a purity of ≥97%. All other chemicals were purchased from Carl Roth (Karlsruhe, Germany), Sigma-Aldrich (St. Louis, Missouri) or VWR (Radnor, Pennsylvania).

Site-directed mutagenesis and RNA synthesis. We used wild type rat ASIC3 cDNA contained in the expression vector pRSSP (Chen et al., 2006b). Mutants of ASIC3 were generated by site-directed mutagenesis following the Stratagene QuikChange protocol; PCR was performed with KAPA HiFi Polymerase (Kapa Biosystems; Wilmington, Massachusetts). The sequences of mutated cDNAs was entirely verified by sequencing (Eurofins Genomics, Ebersberg, Germany).

After linearization of plasmids with Mlu I (NEB Biolabs, Ipswich, USA), capped cRNA was synthesized using the mMessage mMachine SP6 transcription kit (Thermo Fischer Scientific, Waltham, Massachusetts, USA). Finally, cRNA was purified using the RNA Clean & Concentrator (Zymo Resarch, Irvine, California, USA). Concentrations were determined with a Nanodrop 2000 spectrophotometer (Thermo Fischer Scientific). RNA was stored at -80°C.

Preparation and injection of oocytes. Animal care and experiments were conducted according to protocols approved by the state office for nature, environment and consumer protection (LANUV) of the state North Rhine-Westphalia (NRW). Surgical removal of ovaries of female *Xenopus laevis* frogs was described previously (Springauf and Gründer, 2010). Oocytes were separated and the follicular membrane was removed by mechanical dissection followed by enzymatic digestion for a period of 2 h with collagenase type 2 (Worthington Biochemical Corporation, Lakewood, NJ, USA). We injected oocytes of stages IV and V with 3 ng capped

Molecular Pharmacology Fast Forward. Published on July 16, 2018 as DOI: 10.1124/mol.118.112375
This article has not been copyedited and formatted. The final version may differ from this version.

cRNA of ASIC3 wt or ASIC3 mutants. For ASIC3 mutated at residues E239 or E79 and for substitutions by cysteine, 8 - 16 ng cRNA were injected. Injected oocytes were incubated for 24 - 72 h at 19°C in oocyte ringer (OR-2; in mM: 82.5 NaCl, 2.5 KCl, 1.0 Na2HPO4, 5.0 HEPES, 1.0 MgCl2, 1.0 CaCl2, 0.5 g/liter polyvinylpyrrolidone, 1,000 U/l penicillin and 10 mg/l streptomycin; pH was adjusted to pH 7.3).

Electrophysiology. For most experiments, we used the Screening Tool (npi electronic, Tamm, Germany) as measurement setup, which provides a small recording chamber combined with a computer-driven dispensing robot, allowing fast and programmable solution exchange (Baburin et al., 2006). Two-electrode voltage clamp (TEVC) recordings of *Xenopus* oocytes were conducted at ambient temperature (20-23°C). A Turbo TEC-03X amplifier (npi electronic) was used to establish voltage clamp conditions at -70 mV in all experiments. Micropipettes filled with 3M KCl and a resistance of 0.5-2 MΩ were used to gain electrical access to oocytes. The current signal was filtered at 20 Hz and digitized with a sampling rate of 500 Hz using the software Cellworks (npi electronic).

For the experiments reported in Fig. 1, a setup with a larger recording chamber and a computer-controlled valve-driven solution exchange system was used. This setup allowed shorter intervals between solution applications (as short as 2 sec) (Madeja et al., 1995). For these experiments, currents were digitized with a sampling rate of 200 Hz.

Bath solutions for TEVC recordings contained (in mM) 140 NaCl, 1.8 $CaCl_2$, 1.0 $MgCl_2$, 10 HEPES (for pH ≥6.6) or 10 MES (for pH <6.6); pH was adjusted with NaOH. If not stated otherwise, pH 7.4 was used as conditioning solution. Compounds were added to the bath solution as indicated.

Photo affinity labelling of ASIC3 by RPR[azF]a. ASIC3-expressing oocytes were incubated in OR-2 medium containing either 30-100 µM RPR[azF]a or 100 µM RPRFa and were

Molecular Pharmacology Fast Forward. Published on July 16, 2018 as DOI: 10.1124/mol.118.112375
This article has not been copyedited and formatted. The final version may differ from this version.

immediately irradiated by UV light. Irradiation was for 1 – 10 min with UV-light of 302 nm in a Gel Doc XR UV-transilluminator (Bio-Rad, Hercules, California, USA). Electrophysiological recordings of photo-crosslinked ASIC3-expressing oocytes were conducted within 2 h after photo-crosslinking.

Data Analysis. For analysis of current recordings, we used Cellworks Reader (npi Electronic, version 6.2.2) and IgorPro (WaveMetrics, version 5.0.3.0; Lake Oswego, Oregon). For kinetic analysis of the current decay phase, it was fit with a double exponential function:

$$I(t) = y_0 + A\,[a_1\, e^{(-t/\tau 1)} + a_2\, e^{(-t/\tau 2)}].$$

I(t) represents the current at time point t, y_0 a sustained current component, A the desensitising current component and a_1 and a_2 the two fractions of current components desensitizing with fast τ_1 and slower τ_2, respectively; $a_1 + a_2 = 1$. The underlying assumption is that currents of ASIC3 with no RPRFa bound decay with τ_1 and currents of ASIC3 with RPRFa bound with τ_2 (Reimers, 2017).

To determine τ after photo-crosslinking with 100 μM RPR[azF]a (Fig. 1), we used a single exponential function. To analyse desensitisation of mutants of the NPLSD (Fig. 6), we first obtained τ_1 for each mutant by fitting with a single exponential function ($a_2 = 0$) current decay in the absence of RPRFa. We then fitted current decay in the presence of RPRFa with a double exponential function, with τ_1 fixed to the value obtained in the absence of RPRFa, yielding mutant-specific a_2 and τ_2. All exponential fits were visually checked and inappropriate fits (e.g. with a negative time constant) were rejected.

Statistical analysis was performed in Excel 2016 (Microsoft, Redmond, WA) and R 3.4.2 (R Core Team, Vienna, Austria). Results are reported as the mean ± S.E.M. Student's unpaired *t* test was used to determine *P* values, except for experiments reported in figure 1, for which Student's paired *t* test was used. Significance levels were defined as follows: $*p < 0.05$, $**p < 0.01$, $***p < 0.001$. In case of multiple testing on the same data set, the Bonferroni

Molecular Pharmacology Fast Forward. Published on July 16, 2018 as DOI: 10.1124/mol.118.112375
This article has not been copyedited and formatted. The final version may differ from this version.

correction was used by multiplying the *P* value by the number of tests. Graphs and current traces were plotted with IgorPro and arranged with Adobe Illustrator CS6. All experiments were conducted with oocytes of at least two different frogs, except photo-labelling experiments which were conducted with oocytes of one frog.

Modelling of rat ASIC3 and RPRFa. We created a knowledge-based homology model of rat ASIC3 (UniProtKB: O35240, 533 aa) in both its open and desensitized state, based on the corresponding ion channel structures of chicken ASIC1a (cASIC1). The sequences were aligned with ClustalW, revealing a sequence identity of 44%. In the open cASIC1 structure, the channel is in complex with the snake toxin MitTx (PDB Entry Code: 4NTW; resolution of 2.07 Å) (Baconguis et al., 2014). For the desensitized receptor state, we used as a template the desensitized structure of cASIC1 (PDB Entry Code: 2QTS; resolution of 1.9 Å) (Jasti et al., 2007).

The full biological assemblies were retrieved from the PDB and processed with Schrödinger software (Maestro Version 11.4.011; Small-Molecule Drug Discovery Suite 2017-4, Schrödinger, LLC, New York), using default settings unless otherwise noted. All entities not belonging to the receptor trimer were removed, and missing side chains/loops were modeled. With PROPKA we adjusted the pH of the receptors to 6, to account for the pH experienced by an open channel. Homology models are provided in Supplemental Fig. 1 and Supplemental Fig. 2 in Protein Data Bank format (pdb). The tetrapeptide RPRF was built from the sequence in an extended conformation and a C-terminal amid group was manually introduced yielding RPRFa.

Binding Site Assessment, Docking, and Scoring of RPRFa Binding Poses. *Binding site.* To characterize potential binding sites on the homology models corresponding to the open and the desensitized states, we used Schrödinger SiteMap (Halgren, 2009). Site candidates were ranked based on SiteScore (see Supplemental Table 2), which considers the presence of hydrophilic

Molecular Pharmacology Fast Forward. Published on July 16, 2018 as DOI: 10.1124/mol.118.112375
This article has not been copyedited and formatted. The final version may differ from this version.

and -phobic features and pocket size. The required amount of enclosure and threshold for van der Waals interactions was decreased to detect also shallower binding sites which are known to be relevant in protein-protein interactions. SiteScore allows ranking of potential binding sites but does not allow predictions concerning the relevance of these sites for a specific ligand.

Docking protocol and scoring. A peptide-protein docking approach as implemented in Schrödinger Glide was performed (Friesner et al., 2006). The centroid of the interaction points in SiteMap served to center a Glide grid, suitable for peptide docking. This grid represents a cubic box (8000 $Å^3$) which encapsulates the lower half of the three palm domains with one cube face positioned approximately parallel to the membrane plane. RPRFa docking was carried out with a standard-precision (SP) docking suite tailored for peptide ligands, SP-peptide (Tubert-Brohman et al., 2013), which ensures sufficient conformational sampling of the peptide. The Glide docking procedure penalizes ligand-receptor interactions producing steric clashes. Moreover, side chains of the receptor were allowed to relax their conformation around the docked ligand. Therefore, none of the binding poses had steric clashes. We scored the resulting binding poses with Glide Emodel (Friesner et al., 2006) since force field terms are particularly well suited to rank individual ligand conformers, rather than different ligands. A homology model of ASIC3 in its open conformation in complex with the best ranked docking pose of RPRFa is provided in Supplemental Fig. 3 in Protein Data Bank format (pdb). A protein-ligand interaction fingerprint (PLIF) was generated with MOE (Molecular Operating Environment, 2013.08; Chemical Computing Group ULC, Montreal, Canada).

Molecular Pharmacology Fast Forward. Published on July 16, 2018 as DOI: 10.1124/mol.118.112375
This article has not been copyedited and formatted. The final version may differ from this version.

Results

RPRFa has to unbind before ASIC3 desensitises. To describe the interaction of RPRFa with ASIC3, Reimers et al. proposed a simplified kinetic model with three sequential states: closed (C), open (O) and desensitized (D) (Fig. 1A). According to this model, RPRFa binds to all of these three states with varying dissociation constants (Reimers et al., 2017). The slower desensitisation in the presence of RPRFa is then explained by a slower transition rate (τ_2) from O_R to D_R, when RPRFa is bound. An alternative explanation would be that RPRFa has to unbind before the channel can desensitize. The slower desensitisation in the presence of RPRFa would then be explained by the transition from O_R to O, which would be significantly slower than the transition from O to D (Fig. 1A), leading to an indirect slowing of desensitization. The main difference between these two explanations is the existence of a desensitized conformation that has RPRFa bound (D_R state), which should be readily populated according to the first explanation, but not according to the second explanation. To decide between these two explanations, we therefore tested the population of the D_R state.

First, we examined whether RPRFa can bind to the desensitized conformation D of ASIC3. We desensitised ASIC3 with pH 6.0 and then applied 100 μM RPRFa for 60 sec at pH 6.0. Next, we washed-out the peptide by two short wash steps (pH 6.0 followed by pH 7.4, 2 sec each). When we then activated ASIC3 by application of pH 6.0, we observed no slowing of desensitization, as measured by the ratio of the current 2.5 sec post peak ($I_{2.5s}$) to the current at peak ($I_{2.5s}/I_{peak}$ = 1.8 ± 0.2% for peak iii and $I_{2.5s}/I_{peak}$ = 2.7 ± 0.4% for peak ii; iii vs. ii, P = 0.26; n = 12; Fig. 1 B). In contrast, when we applied RPRFa for 60 sec at pH 7.4, followed by two wash steps of identical duration as before (pH 7.4, 2 sec each), desensitization of ASIC3 after activation by pH 6.0 was strongly slowed down ($I_{2.5s}/I_{peak}$ = 71 ± 13% for peak iv; iv vs iii; $P < 0.001$; Fig. 1B). We conclude that the affinity for RPRFa of the desensitized state D is much smaller than of the closed state C, either due to a smaller binding rate or due to a larger unbinding rate.

Molecular Pharmacology Fast Forward. Published on July 16, 2018 as DOI: 10.1124/mol.118.112375
This article has not been copyedited and formatted. The final version may differ from this version.

Next, we tested whether RPRFa unbinds during current decline (Fig. 1C). We pre-applied RPRFa (30 μM, 60 sec) and then activated ASIC3 for 17 sec with pH 6.0 in the absence of RPRFa. During this long activation current declined to <20% of its peak amplitude. It was followed by a short 2 sec-interval in pH 7.4 (no RPRFa), just enough to allow recovery of ASIC3. We then activated again with pH 6.0 and evaluated current decline. In case RPRFa stayed bound to ASIC3 during the long first current decline, the slowly desensitizing current component of the second activation should be larger than the current at the end of the previous activation. In contrast, in case RPRFa unbound during current decline, the slowly desensitizing current component of the second activation should be similar to or smaller than the current at the end of the previous activation. We found that the slowly desensitizing current component of the second activation was indeed similar to the current at the end of the previous activation (Fig. 1C, left panel). To rule out that RPRFa unbinding happened during the 2 sec interval at pH 7.4, we pre-applied RPRFa as before (60 sec), followed by 2 sec pre-conditioning at pH 7.4 in the absence of RPRFa. When we then activated with pH 6.0 and evaluated $I_{2.5s}/I_{peak}$, we found that channels were strongly modified ($I_{2.5s}/I_{peak}$ = 47.8 ± 2.4%; n = 7). Although $I_{2.5s}/I_{peak}$ was larger without the 2 sec-interval at pH 7.4 ($I_{2.5s}/I_{peak}$ = 60.6 ± 2.6%, peak i; n = 9; iii vs. i, P = 0.004), this result still rules out that RPRFa unbinds quickly at pH 7.4, suggesting that current decline of ASIC3 after RPRFa-modification is accompanied by a substantial unbinding of RPRFa.

So far, we found no evidence that the desensitised conformation with RPRFa bound (D_R) is strongly populated. If RPRFa indeed needs to unbind to allow desensitization of ASIC3, the irreversible binding of RPRFa should prevent desensitization of ASIC3. To test this prediction, we replaced the F residue of RPRFa by the photo-reactive unnatural amino acid 4-Azido-L-phenylalanine (AzF) to yield RPR[azF]a. Upon irradiation by UV light, the azide moiety of AzF is converted to the highly reactive nitrene group, which allows the covalent attachment of RPR[azF]a to ASIC3.

Molecular Pharmacology Fast Forward. Published on July 16, 2018 as DOI: 10.1124/mol.118.112375
This article has not been copyedited and formatted. The final version may differ from this version.

RPR[azF]a slowed desensitization of ASIC3 similar to RPRFa (Fig. 2A), even with a higher apparent affinity and a slower τ_{des} than RPRFa (EC_{50}: 1.2 ± 0.2 μM; τ_{des} = 12.1 ± 3 s; n = 7; Fig. 2A) (Reimers et al., 2017), demonstrating that the peptide containing the AzF modification still binds to and modifies ASIC3. We then irradiated ASIC3-expressing oocytes with UV light for 1-10 minutes in 30-100 μM peptide (Fig. 2B). As control, we irradiated ASIC3-expressing oocytes with UV light for 6 min in the presence of 100 μM unmodified RPRFa. When cells treated with RPR[azF]a were subsequently activated by pH 6.0, a sustained current was observed, although no peptide was present or pre-applied (Fig. 2C). This sustained current was not observed for control oocytes that had been incubated in RPRFa, suggesting that RPR[azF]a was covalently bound to ASIC3 and modulated the channel. The sustained current increased with increasing durations of photo labelling (I_{25s}/I_{peak} ratios: control, 0.3 ± 0.2%; UV-treatment 1 min, 3.7 ± 0.4%; UV 6 min, 20.5 ± 1.8%; UV 10 min, 59.8 ± 5.0%; $P < 0.001$ for all conditions with UV-treatment; n = 5-10; Fig. 2D). But in contrast to modulation by RPRFa, the sustained current of covalently modulated channels persisted for the whole duration of pH 6.0 application (30 sec) without any apparent desensitization. Moreover, the transient part of the current desensitized with a τ_{des} that is typical for unmodified ASIC3; only at prolonged UV irradiation, τ_{des} was slowed down (τ_{des}: control, 0.44 ± 0.02 sec; UV-treatment 1 min, 0.62 ± 0.06 sec, P = 0.08; UV 6 min, 0.82 ± 0.07 sec, P = 0.004; UV 10 min, 1.43 ± 0.14 sec, P = 0.005). These results are expected when UV irradiation leads to two populations of ASIC3, one covalently modified by RPRFa and one unmodified. The modified population would be trapped in the open conformation (O-R) and would not desensitize at all, and the other fraction would desensitize with the usual τ_{des}. The increase in the sustained current with increasing duration of UV irradiation speaks in favor of this interpretation.

To further test the presence of two populations (one covalently modified and one unmodified) in these experiments, we irradiated ASIC3-expressing oocytes with UV light for 4 min in 30 μM RPR[azF]a. As before, these oocytes displayed a non-desensitising sustained

Molecular Pharmacology Fast Forward. Published on July 16, 2018 as DOI: 10.1124/mol.118.112375
This article has not been copyedited and formatted. The final version may differ from this version.

current when subsequently activated by pH 6.0. Importantly, the transient current was still sensitive to RPR[azF]a (no UV irradiation), which slowed desensitization similar to RPRFa (Fig. 2E). Thus, this result is in agreement with two populations of ASIC3 in UV-irradiated oocytes that had been incubated in RPR[azF]a.

Collectively, these results strongly argue that RPRFa has to unbind before ASIC3 can desensitize and that the kinetics of current decline of ASIC3 in the presence of RPRFa mainly reflects the slow unbinding of RPRFa (transition O_R to O, Fig. 1A).

Molecular docking predicts the nonproton ligand-sensing domain as a possible binding site for RPRFa. To discover possible binding sites of RPRFa on ASIC3, we modelled the open and the desensitized conformations of rat ASIC3 on the open and the desensitized conformation of chicken ASIC1, respectively (PDB ID: 4NTW and 2QTS, see methods for further details). We then performed an unbiased binding sites detection protocol (see methods for detail) across these two *in silico* models and found several potential binding sites; for each model, the five highest ranking sites according to SiteScore are reported in Supplemental table 1. Since experimental evidence, as reported above, suggests that RPRFa unbinds before ASIC3 desensitizes, the binding site of RPRFa should be located in a region only accessible in the open state but not in the desensitized state. The largest binding site, in the open-state model, which is not accessible in the desensitized state model, is a cavity in the lower palm domain, the NPLSD. Indeed, in cASIC1 the lower palm domain slightly shrinks on passing from the open to the desensitized state (Baconguis and Gouaux, 2012) and this is also reflected in our models. The conformational changes in the lower palm domain, when transitioning from open to the desensitized state, suggest that RPRFa binding to the NPLSD might be sterically unfavorable in the desensitized state.

RPRFa was therefore docked into the NPLSD of the open-state homology model of ASIC3 (Fig. 3). Protein–peptide docking is more challenging than small molecule docking,

Molecular Pharmacology Fast Forward. Published on July 16, 2018 as DOI: 10.1124/mol.118.112375
This article has not been copyedited and formatted. The final version may differ from this version.

since even short peptides are often highly flexible, and several binding poses with comparable probability are possible. We obtained 34 distinct binding poses (Supplemental table 2). These are summarized by a Protein Ligand Interaction Fingerprint (PLIF) showing the interaction between RPRFa and ASIC3 (Fig. 4 and Supplemental Fig. 4). High-ranking poses form cation-π interactions with the C-terminal F of RPR**F**a and R376 in β-strand 10, while the amid capping group hydrogen bonds with Q269 of β9. Salt bridges can be observed between the C-terminal R of RP**R**Fa and E79/E423 as well as for the N-terminal R of **R**PRFa and E418 (Fig. 4A). Notably, the interactions between the peptide and receptor can involve more than one monomer at the same time (Supplemental Fig. 4), possibly altering monomer interaction. Supplemental Fig. 3 provides the homology model of ASIC3 in its open conformation in complex with RPRFa in its best-ranked docking pose and supplemental Fig. 5 provides a movie of this complex.

The nonproton ligand sensing domain is involved in modulation by RPRFa. The NPLSD is mainly encapsulated by four β-strands of each of the three palm domains (Jasti et al., 2007). To test experimentally the prediction by *in silico* docking, we substituted by different other amino acids eight residues in the NPLSD that surrounded RPRFa docked to the homology model: L77 and E79 in β-strand 1, E423 in β12, Q269 and Q271 in β9, and R376, A378, and E380 in β10 (total of 23 mutations; Fig. 5 and Supplemental Table 3). First, we activated ASIC3 wild type and each mutant with pH 6.3 and pH 4.0 and then pre-applied 3 μM RPRFa followed by another activation with pH 6.3 (Fig. 5B). To quantify modulation by RPRFa, we calculated the difference of the current remaining after 2.5 sec with and without RPRFa ($I_{2.5s+RFa} - I_{2.5s-RFa}$) and normalized it to the peak current ($[I_{2.5s+RFa} - I_{2.5s-RFa}]/I_{Peak-RFa}$). Out of a total of 23 mutants, for 18 mutants $[I_{2.5s+RFa} - I_{2.5s-RFa}]/I_{Peak-RFa}$ was significantly reduced, compared to the wild type (Fig. 5C and Supplemental Table 3). Notably, all substitutions of R376 and Q269, two amino acids that appeared to be crucial for interaction with the Famide group of RPRFa in *in silico* docking (Fig. 4), significantly reduced modulation by RPRFa. Similarly, substitutions

Molecular Pharmacology Fast Forward. Published on July 16, 2018 as DOI: 10.1124/mol.118.112375
This article has not been copyedited and formatted. The final version may differ from this version.

of E423, which makes extensive contacts to RPRFa in most docking poses (Fig. 4B), also significantly reduced modulation by RPRFa, with the exception of the relatively conservative exchange E423Q (Fig. 5D). As an alternative way to quantify modulation by RPRFa, we also calculated the ratio $I_{2.5s+RFa}/I_{2.5s-RFa}$. Also in this type of analysis, 17 out of the 23 mutations in the NPLSD, including all substitutions of R376 and Q269, significantly reduced modulation by RPRFa (Supplemental Fig. 6 and Supplemental Table 3). Together, these results show that the NPLSD is crucial for the modulation of ASIC3 by RPRFa. To test whether the mutations specifically changed the interaction of amino acids of the NPLSD with RPRFa, we additionally generated mutants Q270E and K379E, which are also located on β-strands 9 and 10 but the side chains of which point away from the cavity to which RPRFa was docked. Both mutants did indeed not significantly affect the modulation by RPRFa as measured by the ratio $[I_{2.5s+RFa} - I_{2.5s-RFa}]/I_{Peak-RFa}$ (Fig. 5C and Supplemental Table 3). For K379E, the ratio $I_{2.5s+RFa}/I_{2.5s-RFa}$ was reduced, albeit less strongly than for the other mutants (Supplemental Fig. 6 and Supplemental Table 3). The results are in agreement with the interpretation that RPRFa was bound to the NPLSD.

Evidence that mutants within the nonproton ligand sensing domain reduce binding of RPRFa and fasten unbinding. In principle, there are two ways by which the mutations might have reduced the modulation by RPRFa: first, by reducing binding or second, by reducing the effect of binding on desensitization. To further differentiate between these two possibilities, for 12 mutants we also tested a higher RPRFa concentration (100 μM) (Fig. 6); for wild type ASIC3, 100 μM RPRFa is a saturating concentration (Reimers, 2017). When looking at a shorter time scale (0.5 sec after peak), RPRFa was indeed able to modulate desensitization kinetics of many mutants (Fig. 6B). To quantify RPRFa effects, we determined $[I_{0.5s+RFa} - I_{0.5s-RFa}]/I_{Peak-RFa}$. For wild type ASIC3 this ratio was 0.90 ± 0.07, whereas it was significantly reduced to a range of -0.10 to 0.51 for 11 mutants (L77F, L77C, E79S, E423R, Q269R, Q269C,

Molecular Pharmacology Fast Forward. Published on July 16, 2018 as DOI: 10.1124/mol.118.112375
This article has not been copyedited and formatted. The final version may differ from this version.

Q271R, R376E, A378R, A378C, and E380Q; Fig. 6C and Supplemental Table 4), confirming the importance of these amino acids for RPRFa modulation of ASIC3.

We then fitted current decay after RPRFa-application by double exponential fits. We fixed the fast time constant τ_1 to the value obtained by a single exponential fit in absence of RPRFa (see Methods) and determined the fraction a_2 and the slow time constant τ_2. This procedure specifically detects and characterizes components of the current decay that are introduced by RPRFa. Since for some mutants, τ_1 was different from wildtype, we analyzed the ratio τ_2/τ_1 to evaluate desensitization in the presence of RPRFa. For wild type ASIC3, 100 μM RPRFa modified 91 ± 3% of the current (a_2) and decelerated desensitisation about 22.0 ± 1.4-fold (τ_2/τ_1; n = 15). In contrast, for L77C, E79S, R376E, A378R and A378C, RPRFa modified a significantly smaller fraction of the current (a_2 ranging from 17% to 67%; Fig. 6D, top, and Supplemental Table 4), which suggests that these mutants had less RPRFa bound. The ratio τ_2/τ_1 was significantly decreased 2.2-11.1-fold for all mutants except for E423R (Fig. 6D, bottom and Supplemental Table 4; Q271R could not be fitted). As outlined above, the speed of current decline in the presence of RPRFa probably reflects unbinding of RPRFa (transition O_R to O; Fig. 1A). A decreased ratio τ_2/τ_1 therefore indicates faster unbinding of RPRFa (smaller τ_2) and, thus, provides another indication that the mutations within the NPLSD reduced affinity of ASIC3 for RPRFa. Taken together, our results reveal the NPLSD as a good candidate for the RPRFa binding site.

The acidic pocket of ASIC3 is not involved in modulation by RPRFa. To further prove that mutations in the NPLSD specifically changed modulation by RPRFa, we made 12 individual amino acid substitutions within the acidic pocket of ASIC3 (Fig. 7A), the binding site of a peptide toxin on ASIC1a (Baconguis and Gouaux, 2012; Dawson et al., 2012) and a highly ranked potential binding site according to SiteScore (see above), and tested their effect on RPRFa modulation (Fig. 7B). In strong contrast to mutations within the NPLSD, none of the

Molecular Pharmacology Fast Forward. Published on July 16, 2018 as DOI: 10.1124/mol.118.112375
This article has not been copyedited and formatted. The final version may differ from this version.

mutations within the acidic pocket significantly reduced the ratio $[I_{2.5s+RFa} - I_{2.5s-RFa}]/I_{Peak-RFa}$ compared to wild type (Fig. 7C). We also calculated the ratio $I_{2.5s+RFa}/I_{2.5s-RFa}$. For the wild type, pre-application of 3 μM RPRFa increased $I_{2.5s}$ 31.7 ± 3.3-fold (n = 102) relative to $I_{2.5s}$ when no RPRFa was pre-applied. For three of the mutants $I_{2.5s+RFa}/I_{2.5s-RFa}$ was significantly decreased (R183E, E212C, and R239E; Supplemental Fig. 7 and Supplemental Table 1). In contrast to an effect on RPRFa modulation, many mutations in the acidic pocket (R183E, M184Y, E212R, E212C, E231R, and R362E) significantly decreased apparent proton affinity as assessed by the ratio $I_{pH6.3}/I_{pH4.0}$ (Supplemental Table 3). Taken together these results suggest that the acidic pocket is not involved in the modulation of ASIC3 by RPRFa, but might be involved in pH sensing.

Discussion

Our results show (i) that RPRFa has to unbind before ASIC3 can desensitize, (ii) that RPRFa docks to the NPLSD of an ASIC3 open state model, and (iii) that mutations within the NPLSD, but not within the acidic pocket, reduce modulation of ASIC3 by RPRFa. The finding that RPRFa has to unbind before ASIC3 can desensitize suggests that the slow time constant τ_2 of the current decay phase, which is introduced by RPRFa (Reimers et al., 2017) and which is commonly described as slower desensitization of ASIC3, in reality reflects unbinding of RPRFa (Fig. 1A). Thus, it appears that RPRFa uses a simple mechanism to modify gating of ASIC3: by stabilizing the open conformation.

Many mutations within the NPLSD, a cavity of the lower palm domain, reduced the modulation of ASIC3 by RPRFa. Mutation of two amino acids that do not point towards the interior of the cavity, however, did not reduce RPRFa modulation. In addition, the reduced a_2 in the bi-exponential fits of mutant ASIC3 and the faster slow time constant τ_2, in our

Molecular Pharmacology Fast Forward. Published on July 16, 2018 as DOI: 10.1124/mol.118.112375
This article has not been copyedited and formatted. The final version may differ from this version.

interpretation indicate reduced binding of RPRFa and faster unbinding of RPRFa, respectively. These findings suggest that RPRFa indeed binds to the NPLSD. In agreement with this idea, the lower palm has been implicated in desensitization by several previous studies (Cushman et al., 2007; Roy et al., 2013; Springauf and Gründer, 2010). In particular, comparison of the open and desensitized conformation revealed that the ECD contracts in the lower palm domain which encapsulates the negatively charged central vestibule (Baconguis et al., 2014), which forms the NPLSD of ASIC3 (Yu et al., 2010). A contraction of the lower palm domain was later confirmed by functional studies; preventing the contraction impairs desensitization (Roy et al., 2013). Moreover, interfering with the conformational changes in the lower palm domain induces sustained currents by destabilizing the desensitized conformation (Springauf and Gründer, 2010). Of particular interest, it has been shown that FRRFa limits covalent modification of a residue in the lower palm domain of ASIC1a (Frey et al., 2013). All these findings are consistent with binding of RPRFa to the NPLSD of ASIC3.

In contrast to mutations within the NPLSD, mutations within the acidic pocket did not reduce modulation of ASIC3 by RPRFa. The acidic pocket has been involved in activation of ASICs by protons (Gründer and Chen, 2010; Jasti et al., 2007; Krauson et al., 2013; Ramaswamy et al., 2013) and binds psalmotoxin 1, a gating modifier toxin that acts like an agonist of ASIC1 (Chen et al., 2005; Chen et al., 2006a). But the acidic pocket has not been implicated in desensitization of ASICs. Our finding that the acidic pocket apparently is not involved in RPRFa modulation is, thus, in agreement with the previous findings on the role of the acidic pocket for ASIC gating.

Collectively, our results are consistent with the following mechanistic model: RPRFa slowly (within several seconds) binds to a cavity in the lower palm domain, the NPLSD, in the closed or the open conformation and sterically stabilizes the open conformation by preventing the contraction of the central vestibule. Unbinding of RPRFa with a time constant on the order of 6 sec (Reimers et al., 2017) would then allow delayed contraction of the central vestibule

Molecular Pharmacology Fast Forward. Published on July 16, 2018 as DOI: 10.1124/mol.118.112375
This article has not been copyedited and formatted. The final version may differ from this version.

and desensitization of ASIC3. Since the time constant of desensitization of ASIC3 (0.3 sec) (Sutherland et al., 2001) is approximately 10-fold faster than unbinding of RPRFa, RPRFa-unbinding would dominate the kinetics of current decay. Although this is a plausible explanation of our results, we can, at present, not exclude other models in which RPRFa binds to a different site than the NPLSD on ASIC3 and, for example, allosterically enhances unbinding of RPRFa. The availability of RPRAzFa as a covalent ligand provides the opportunity to unequivocally determine the binding site of RPRFa on ASIC3 in the future, by identifying the covalently modified channel fragments, for example by tandem MS analysis.

We have previously shown that the prototypical RFamide FMRFa competes with RPRFa for modulation of ASIC3 (Reimers et al., 2017), suggesting that both RFamides share a binding site. Since all RFamides have similar effects on ASICs (Vick and Askwith, 2015), mainly slowing current decay (Askwith et al., 2000; Chen et al., 2005; Deval et al., 2003; Reimers et al., 2017), it is conceivable that all RFamide neuropeptides, which modulate ASICs, share a binding site on ASICs. Thus, the cavity in the lower palm domain is a likely common binding site for RFamide neuropeptides on ASICs. Although RFamides modulate also other ASICs than ASIC3 (Askwith et al., 2000), ASIC3 and ASIC3-containing heteromers seem to be more strongly modulated by RFamides than other ASICs (Chen et al., 2006b; Deval et al., 2003; Vick and Askwith, 2015); RPRFa, in particular, modulates only ASIC3 and different ASIC3-containing heteromers but not ASIC1a (Reimers et al., 2017). It is likely that structural differences in the central vestibule are responsible for the differential sensitivity of different ASICs to RFamides. It might be that RFamides bind with lower affinity to the NPLSD of ASIC1a, for example. Since ASIC1a desensitizes more slowly than ASIC3, an enhanced unbinding of RFamides, due to lower affinity, could result in a situation where the kinetics of current decay would still be dominated by desensitization rather than by RFamide unbinding, effectively reducing the functional outcome of RFamide binding to the channel. Future studies are necessary to reveal the molecular basis for the subtype-specific action of RFamides.

Molecular Pharmacology Fast Forward. Published on July 16, 2018 as DOI: 10.1124/mol.118.112375
This article has not been copyedited and formatted. The final version may differ from this version.

If RFamide neuropeptides indeed bind to the NPLSD of ASIC3 they would add to several other ligands for which there is evidence that they bind to the NPLSD. 2-guanidine-4-methylquinazoline (GMQ) is a synthetic ligand that induces sustained ASIC3 currents already at pH 7.4 (Yu et al., 2010) and also binds to the NPLSD (Yu et al., 2010). Also different natural ligands bind to the NPLSD, such as the arginine metabolite agmatine (Li et al., 2010; Yu et al., 2010), serotonin (Wang et al., 2013) and the pruritogenic peptide SLIGRLamide (Peng et al., 2015). Thus, the NPLSD appears as an important binding cavity in the ECD of ASIC3. All these ligands, including RPRFa, are positively charged, containing guanidine or amine groups, which suggests that they are attracted by the negative charges of the central vestibule (Jasti et al., 2007). Moreover, the presence of two guanidine and one amino group in RPRFa might explain its particularly high affinity for ASIC3 (Reimers et al., 2017), for example compared with FMRFa, which has only one guanidine and one amino group.

Apart from the positive charges of the ligands binding to the NPLSD, their precise structures are quite diverse, however. This situation is reminiscent of the delayed rectifier K^+ channel hERG, where many structurally diverse compounds bind to a common inner cavity to inhibit the channel (Mitcheson et al., 2005). This cavity is particularly large in hERG compared to other related K^+ channels, explaining the drug promiscuity of hERG. Perhaps the central vestibule of ASIC3 is also larger than that of other ASICs explaining its sensitivity to different compounds, some of which are quite bulky. It might be that the central vestibule of ASIC3 evolved to a cavity where different physiological ligands bind to modulate the activity of ASIC3.

In summary, our results reveal how RPRFa slows current decay of ASIC3 and that the NPLSD is important for the modulation of ASIC3 by RPRFa. Although we cannot exclude other models, we propose a mechanistic model in which RPRFa binds to the NPLSD preventing the contraction of the central vestibule which appears to be sufficient to slow desensitization.

Molecular Pharmacology Fast Forward. Published on July 16, 2018 as DOI: 10.1124/mol.118.112375
This article has not been copyedited and formatted. The final version may differ from this version.

Acknowledgments

We thank D. Wiemuth for many helpful discussions.

Molecular Pharmacology Fast Forward. Published on July 16, 2018 as DOI: 10.1124/mol.118.112375
This article has not been copyedited and formatted. The final version may differ from this version.

AUTHOR'S CONTRIBUTIONS

Participated in research design: Schmidt and Gründer.

Conducted experiments: Reiners, Margreiter, Oslender-Bujotzek and Schmidt.

Performed data analysis: Reiners, Margreiter, Schmidt and Rossetti.

Wrote or contributed to writing of the manuscript: Rossetti, Schmidt and Gründer.

Molecular Pharmacology Fast Forward. Published on July 16, 2018 as DOI: 10.1124/mol.118.112375
This article has not been copyedited and formatted. The final version may differ from this version.

References

Askwith CC, Cheng C, Ikuma M, Benson C, Price MP and Welsh MJ (2000) Neuropeptide FF and FMRFamide potentiate acid-evoked currents from sensory neurons and proton-gated DEG/ENaC channels. *Neuron* **26**(1): 133-141.

Baburin I, Beyl S and Hering S (2006) Automated fast perfusion of Xenopus oocytes for drug screening. *Pflugers Arch* **453**(1): 117-123.

Baconguis I, Bohlen CJ, Goehring A, Julius D and Gouaux E (2014) X-ray structure of acid-sensing ion channel 1-snake toxin complex reveals open state of a Na(+)-selective channel. *Cell* **156**(4): 717-729.

Baconguis I and Gouaux E (2012) Structural plasticity and dynamic selectivity of acid-sensing ion channel-spider toxin complexes. *Nature* **489**(7416): 400-405.

Bartoi T, Augustinowski K, Polleichtner G, Gründer S and Ulbrich MH (2014) Acid-sensing ion channel (ASIC) 1a/2a heteromers have a flexible 2:1/1:2 stoichiometry. *Proc Natl Acad Sci U S A*.

Benson CJ, Eckert SP and McCleskey EW (1999) Acid-evoked currents in cardiac sensory neurons: A possible mediator of myocardial ischemic sensation. *Circ Res* **84**(8): 921-928.

Chen X, Kalbacher H and Gründer S (2005) The tarantula toxin psalmotoxin 1 inhibits acid-sensing ion channel (ASIC) 1a by increasing its apparent H+ affinity. *J Gen Physiol* **126**(1): 71-79.

Chen X, Kalbacher H and Gründer S (2006a) Interaction of acid-sensing ion channel (ASIC) 1 with the tarantula toxin psalmotoxin 1 is state dependent. *J Gen Physiol* **127**(3): 267-276.

Chen X, Paukert M, Kadurin I, Pusch M and Gründer S (2006b) Strong modulation by RFamide neuropeptides of the ASIC1b/3 heteromer in competition with extracellular calcium. *Neuropharmacology* **50**(8): 964-974.

Cushman KA, Marsh-Haffner J, Adelman JP and McCleskey EW (2007) A conformation change in the extracellular domain that accompanies desensitization of acid-sensing ion channel (ASIC) 3. *J Gen Physiol* **129**(4): 345-350.

Dawson RJ, Benz J, Stohler P, Tetaz T, Joseph C, Huber S, Schmid G, Hugin D, Pflimlin P, Trube G, Rudolph MG, Hennig M and Ruf A (2012) Structure of the Acid-sensing ion channel 1 in complex with the gating modifier Psalmotoxin 1. *Nat Commun* **3**: 936.

Deval E, Baron A, Lingueglia E, Mazarguil H, Zajac JM and Lazdunski M (2003) Effects of neuropeptide SF and related peptides on acid sensing ion channel 3 and sensory neuron excitability. *Neuropharmacology* **44**(5): 662-671.

Deval E and Lingueglia E (2015) Acid-Sensing Ion Channels and nociception in the peripheral and central nervous systems. *Neuropharmacology* **94**: 49-57.

Deval E, Noel J, Gasull X, Delaunay A, Alloui A, Friend V, Eschalier A, Lazdunski M and Lingueglia E (2011) Acid-sensing ion channels in postoperative pain. *J Neurosci* **31**(16): 6059-6066.

Deval E, Noel J, Lay N, Alloui A, Diochot S, Friend V, Jodar M, Lazdunski M and Lingueglia E (2008) ASIC3, a sensor of acidic and primary inflammatory pain. *The EMBO journal* **27**(22): 3047-3055.

Frey EN, Pavlovicz RE, Wegman CJ, Li C and Askwith CC (2013) Conformational changes in the lower palm domain of ASIC1a contribute to desensitization and RFamide modulation. *PLoS One* **8**(8): e71733.

Friesner RA, Murphy RB, Repasky MP, Frye LL, Greenwood JR, Halgren TA, Sanschagrin PC and Mainz DT (2006) Extra precision glide: docking and scoring incorporating a model of hydrophobic enclosure for protein-ligand complexes. *J Med Chem* **49**(21): 6177-6196.

Gründer S and Chen X (2010) Structure, function, and pharmacology of acid-sensing ion channels (ASICs): focus on ASIC1a. *Int J Physiol Pathophysiol Pharmacol* **2**(2): 73-94.

Gründer S and Pusch M (2015) Biophysical properties of acid-sensing ion channels (ASICs). *Neuropharmacology* **94**: 9-18.

Halgren TA (2009) Identifying and characterizing binding sites and assessing druggability. *J Chem Inf Model* **49**(2): 377-389.

Ikeuchi M, Kolker SJ and Sluka KA (2009) Acid-sensing ion channel 3 expression in mouse knee joint afferents and effects of carrageenan-induced arthritis. *J Pain* **10**(3): 336-342.

Jasti J, Furukawa H, Gonzales EB and Gouaux E (2007) Structure of acid-sensing ion channel 1 at 1.9 A resolution and low pH. *Nature* **449**(7160): 316-323.

Krauson AJ, Rued AC and Carattino MD (2013) Independent contribution of extracellular proton binding sites to ASIC1a activation. *J Biol Chem* **288**(48): 34375-34383.

Li WG, Yu Y, Zhang ZD, Cao H and Xu TL (2010) ASIC3 channels integrate agmatine and multiple inflammatory signals through the nonproton ligand sensing domain. *Mol Pain* **6**: 88.

Madeja M, Musshoff U and Speckmann EJ (1995) Improvement and testing of a concentration-clamp system for oocytes of Xenopus laevis. *Journal of Neuroscience Methods* **63**(1-2): 211-213.

Marra S, Ferru-Clement R, Breuil V, Delaunay A, Christin M, Friend V, Sebille S, Cognard C, Ferreira T, Roux C, Euller-Ziegler L, Noel J, Lingueglia E and Deval E (2016) Non-acidic activation of pain-related Acid-Sensing Ion Channel 3 by lipids. *The EMBO journal* **35**(4): 414-428.

Mitcheson J, Perry M, Stansfeld P, Sanguinetti MC, Witchel H and Hancox J (2005) Structural determinants for high-affinity block of hERG potassium channels. *Novartis Found Symp* **266**: 136-150; discussion 150-138.

Molliver DC, Immke DC, Fierro L, Pare M, Rice FL and McCleskey EW (2005) ASIC3, an acid-sensing ion channel, is expressed in metaboreceptive sensory neurons. *Mol Pain* **1**: 35.

Omori M, Yokoyama M, Matsuoka Y, Kobayashi H, Mizobuchi S, Itano Y, Morita K and Ichikawa H (2008) Effects of selective spinal nerve ligation on acetic acid-induced nociceptive responses and ASIC3 immunoreactivity in the rat dorsal root ganglion. *Brain Res* **1219**: 26-31.

Peng Z, Li WG, Huang C, Jiang YM, Wang X, Zhu MX, Cheng X and Xu TL (2015) ASIC3 Mediates Itch Sensation in Response to Coincident Stimulation by Acid and Nonproton Ligand. *Cell Rep* **13**(2): 387-398.

Ramaswamy SS, MacLean DM, Gorfe AA and Jayaraman V (2013) Proton-mediated conformational changes in an acid-sensing ion channel. *J Biol Chem* **288**(50): 35896-35903.

Reimers C, Lee CH, Kalbacher H, Tian Y, Hung CH, Schmidt A, Prokop L, Kauferstein S, Mebs D, Chen CC and Gründer S (2017) Identification of a cono-RFamide from the venom of Conus textile that targets ASIC3 and enhances muscle pain. *Proc Natl Acad Sci U S A* **114**(17): E3507-E3515.

Ross JL, Queme LF, Cohen ER, Green KJ, Lu P, Shank AT, An S, Hudgins RC and Jankowski MP (2016) Muscle IL1beta Drives Ischemic Myalgia via ASIC3-Mediated Sensory Neuron Sensitization. *J Neurosci* **36**(26): 6857-6871.

Roy S, Boiteux C, Alijevic O, Liang C, Berneche S and Kellenberger S (2013) Molecular determinants of desensitization in an ENaC/degenerin channel. *Faseb J* **27**(12): 5034-5045.

Sluka KA and Gregory NS (2015) The dichotomized role for acid sensing ion channels in musculoskeletal pain and inflammation. *Neuropharmacology* **94**: 58-63.

Sluka KA, Price MP, Breese NM, Stucky CL, Wemmie JA and Welsh MJ (2003) Chronic hyperalgesia induced by repeated acid injections in muscle is abolished by the loss of ASIC3, but not ASIC1. *Pain* **106**(3): 229-239.

Springauf A and Gründer S (2010) An acid-sensing ion channel from shark (Squalus acanthias) mediates transient and sustained responses to protons. *J Physiol* **588**(Pt 5): 809-820.

Sutherland SP, Benson CJ, Adelman JP and McCleskey EW (2001) Acid-sensing ion channel 3 matches the acid-gated current in cardiac ischemia-sensing neurons. *Proc Natl Acad Sci U S A* **98**(2): 711-716.

Tian Y, Bresenitz P, Reska A, El Moussaoui L, Beier CP and Gründer S (2017) Glioblastoma cancer stem cell lines express functional acid sensing ion channels ASIC1a and ASIC3. *Sci Rep* **7**(1): 13674.

Tubert-Brohman I, Sherman W, Repasky M and Beuming T (2013) Improved docking of polypeptides with Glide. *J Chem Inf Model* **53**(7): 1689-1699.

Vick JS and Askwith CC (2015) ASICs and neuropeptides. *Neuropharmacology* **94**: 36-41.

Wang X, Li WG, Yu Y, Xiao X, Cheng J, Zeng WZ, Peng Z, Xi Zhu M and Xu TL (2013) Serotonin facilitates peripheral pain sensitivity in a manner that depends on the nonproton ligand sensing domain of ASIC3 channel. *J Neurosci* **33**(10): 4265-4279.

Yagi J, Wenk HN, Naves LA and McCleskey EW (2006) Sustained currents through ASIC3 ion channels at the modest pH changes that occur during myocardial ischemia. *Circ Res* **99**(5): 501-509.

Yu Y, Chen Z, Li WG, Cao H, Feng EG, Yu F, Liu H, Jiang H and Xu TL (2010) A nonproton ligand sensor in the acid-sensing ion channel. *Neuron* **68**(1): 61-72.

Molecular Pharmacology Fast Forward. Published on July 16, 2018 as DOI: 10.1124/mol.118.112375
This article has not been copyedited and formatted. The final version may differ from this version.

Footnotes

Please address reprint requests to: Stefan Gründer, Institute of Physiology, RWTH Aachen University, Pauwelsstrasse 30, D-52074 Aachen, Germany, E-mail: sgruender@ukaachen.de

Molecular Pharmacology Fast Forward. Published on July 16, 2018 as DOI: 10.1124/mol.118.112375
This article has not been copyedited and formatted. The final version may differ from this version.

Figure Legends

Fig. 1. The desensitized state of ASIC3 with RPRFa bound is not strongly populated. (A) Simplified kinetic model of the three main states of ASIC3 with or without RPRFa bound. τ_1 and τ_2 are the time constants of current decay in the absence or presence of RPRFa. The transitions that describe current decay are highlighted in bold. State D_R is highlighted as its population is unsure. (B) Left, representative current trace of ASIC3-expressing oocytes when activated by pH 6.0 (black bars) and treated with 100 μM RPRFa (red bars). Peaks are marked by roman numerals. Right, mean $I_{2.5\ sec}/I_{peak}$ ratios for the pH-activated currents. Mean absolute current of peak i was -17.4 ± 3.4 μA; n = 12. (C) Left, representative current trace of ASIC3-expressing oocytes when activated by pH 6.0 (black bars) and treated with 30 μM RPRFa (red bars). Peaks are marked by roman numerals. The dotted red line represents a fit of the current decline of peak i. Current decline of peak ii followed this fit. The trace shown is representative for nine similar experiments. Right, mean $I_{2.5\ sec}/I_{peak}$ ratios. Mean absolute current of peak i was -14.0 ± 5.1 μA; n = 9. Error bars represent S.E.M.; **, $P < 0.01$; ***, $P < 0.001$ (Student´s paired *t* test).

Fig. 2. The photoreactive peptide RPR[azF]a abolishes desensitization when cross-linked to ASIC3. (A) Left, representative current trace illustrating that increasing concentrations of RPR[azF]a (red bars) slow the desensitisation and increase current amplitude of ASIC3 activated by pH 6.3 (black bars). Right, concentration-response curve. The response was quantified as the $I_{5\ sec}/I_{peak}$ ratio in measurements like the one shown on the left. n = 7 for 1 μM, 10 μM and 100 μM and n = 5 for 0.1 μM, 3 μM and 30 μM. (B) Scheme illustrating that ASIC3 expressing oocytes were incubated in RPR[azF]a and irradiated by UV-light. Irradiation time and RPR[azF]a concentration were 1 min and 30 μM, 6 min and 100 μM, or 10 min and 30 μM. When applied for 10 min, half of the RPR[azF]a solution was renewed every 2 min. The control condition was incubated in 100 μM RPRFa and irradiated for 6 min. (C) Representative

Molecular Pharmacology Fast Forward. Published on July 16, 2018 as DOI: 10.1124/mol.118.112375
This article has not been copyedited and formatted. The final version may differ from this version.

ASIC3 expressing oocytes, which had been photo-labelled, were activated by pH 6.0 (black bar) in the absence of any peptide. (D) Mean $I_{25\ sec}/I_{peak}$ ratios of pH 6.0 currents of UV-irradiated ASIC3 expressing oocytes. n = 5-10. Error bars represent S.E.M.; *** = $P < 0.001$. Mean absolute peak currents were in the range of -7.0 ± 3.1 μA to -17.0 ± 2.5 μA. (E) Representative current trace of an ASIC3 expressing oocyte, which had been photo-labelled with 30 μM RPR[azF]a for 4 min. The first activation with pH 6.0 was in the absence of peptide and the second activation was after pre-application of 30 μM RPR[azF]a. Six similar measurements were recorded in the same week.

Fig. 3. Cartoon representation of ASIC3 in complex with RPRFa. (A) Top view. (B) Side view with one monomer removed; highest ranked RPRFa docking pose in green licorice. The cartoon was made with PyMol (The PyMOL Molecular Graphics System, Version 2.0 Schrödinger, LLC). (C) Higher magnification view of the highest ranked docking pose with key interactions highlighted.

Fig. 4: Binding of RPRFa to the NPLSD of ASIC3. (A) 2D protein-ligand interaction diagram of the best binding pose. (B) Protein-ligand interaction fingerprint (PLIF) in population representation. For each amino acid of the receptor as many columns are displayed as there are distinguishable non-covalent interactions in at least one pose. The individual scores are provided in Supplemental Table 2 and the barcode representation in Supplemental Fig. 1.

Fig. 5. Mutation of residues in the NPLSD reduce the modulation by RPRFa. (A) Scheme illustrating the four β strands of one subunit that surround the cavity in the lower palm domain. Approximate positions of amino acids that point towards the cavity and have been mutated are indicated. (B) Representative current trace of an ASIC3-expressing oocyte when activated by pH 6.3 (black bar) or pH 4.0 (blue bar) with or without pre-application of RPRFa (3 μM, red

Molecular Pharmacology Fast Forward. Published on July 16, 2018 as DOI: 10.1124/mol.118.112375
This article has not been copyedited and formatted. The final version may differ from this version.

bar). (C) Representative pH-activated currents of NPLSD mutants in the absence of (black trace) and after pre-incubation with (red trace) 3μM RPRFa were overlaid. (D) Mean [$I_{2.5s+RFa} - I_{2.5s-RFa}$]/$I_{Peak-RFa}$ ratios for all 25 mutants of the NPLSD. Bars are shown in the colour of the corresponding β strands in A; the white bars represent residues whose side chains point away from the cavity. Error bars indicate SEM. n_{mutant} = 8-19; n_{wt} = 4-28 (each condition), n_{wt} (total) = 102. *, $P < 0.05$; **, $P < 0.01$; ***, $P < 0.001$ (Student´s t-test followed by Bonferroni correction).

Fig. 6. Mutations within the NPLSD are affected by high concentrations of RPRFa. (A) Representative recording of an ASIC3 expressing oocyte, illustrating the application protocol. ASIC3 was first activated by pH 6.3 (black bar) without peptide and then after pre-application of 100 μM RPRFa (red bar). (B) Representative pH-activated currents of NPLSD mutants in the absence of (black trace) and after pre-incubation with (red trace) 3μM RPRFa were overlaid. Grey vertical lines indicate the time points 0, 0.5 and 2.5 sec post peak. (C) Bar graph displaying mean ratios of current amplitudes 0.5 sec post-peak in the presence and in the absence of RPRFa ([$I_{0.5s+RFa} - I_{0.5s-RFa}$]/$I_{Peak-RFa}$). Error bars indicate SEM; n_{wt} = 17, n_{mutant} = 6-12. (D) Current decay after pre-application of RPRFa was fit with double exponential functions yielding a_2 (top) and the ratio τ_2/τ_1 (bottom). Mutant Q271R was not analysed, because it could not be fit properly. n_{wt} = 15, n_{mutant} = 6-10. *, $P < 0.05$; **, $P < 0.01$; ***, $P < 0.001$.

Fig. 7. Mutation of residues in the acidic pocket do not impair modulation by RPRFa. (A) Scheme of the topology of the acidic pocket of ASIC3. (B) Top, pH 6.3-activated currents with (red trace) or without (black trace) 3 μM RPRFa were taken from recordings as the one shown in Fig. 5B and overlaid. Bottom, bar graph showing mean ratios [$I_{2.5s+RFa} - I_{2.5s-RFa}$]/$I_{Peak-RFa}$ for the 14 mutants of the acidic pocket. The dotted line represents the ratio of the wild type as reference. Error bars indicate SEM. n_{mutant} = 8-18; n_{wt} = 6-20 (each condition), n_{wt} (total) = 102.

Molecular Pharmacology Fast Forward. Published on July 16, 2018 as DOI: 10.1124/mol.118.112375
This article has not been copyedited and formatted. The final version may differ from this version.

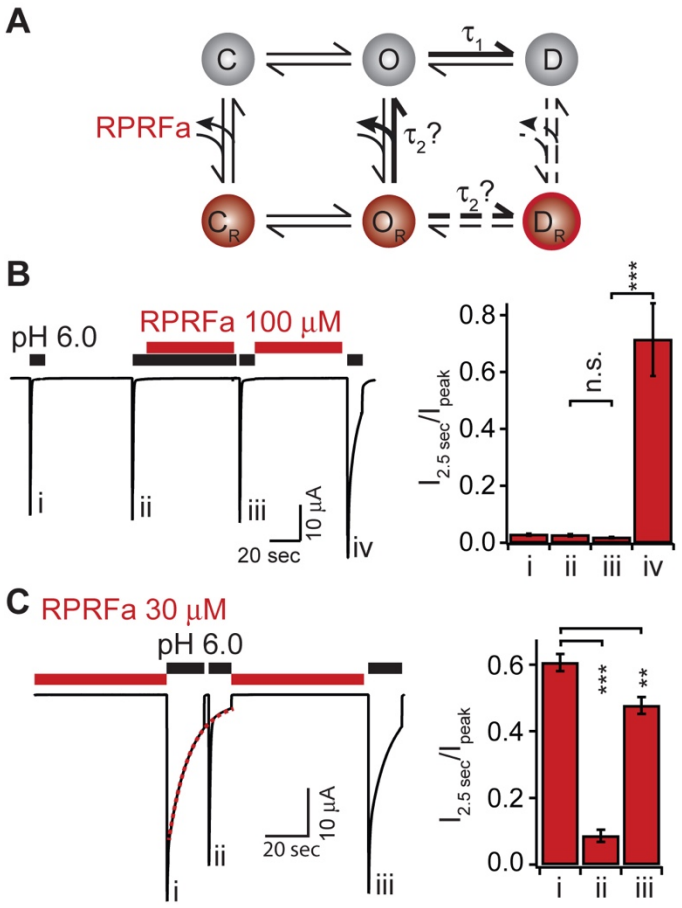

Figure 1

Molecular Pharmacology Fast Forward. Published on July 16, 2018 as DOI: 10.1124/mol.118.112375
This article has not been copyedited and formatted. The final version may differ from this version.

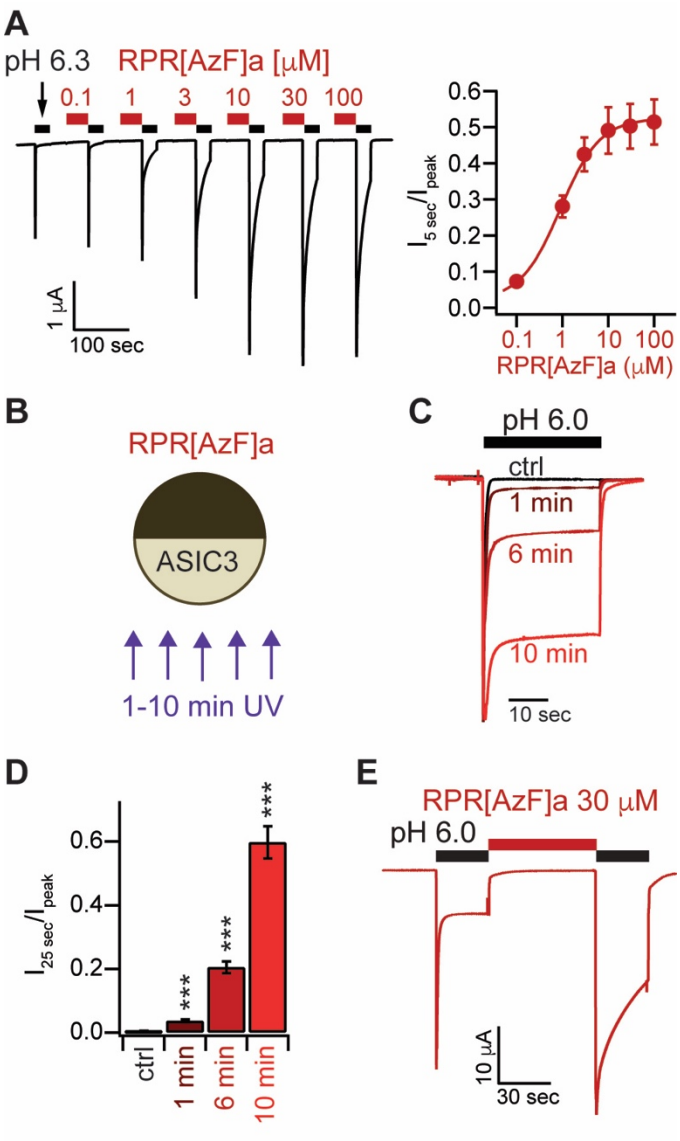

Figure 2

Molecular Pharmacology Fast Forward. Published on July 16, 2018 as DOI: 10.1124/mol.118.112375
This article has not been copyedited and formatted. The final version may differ from this version.

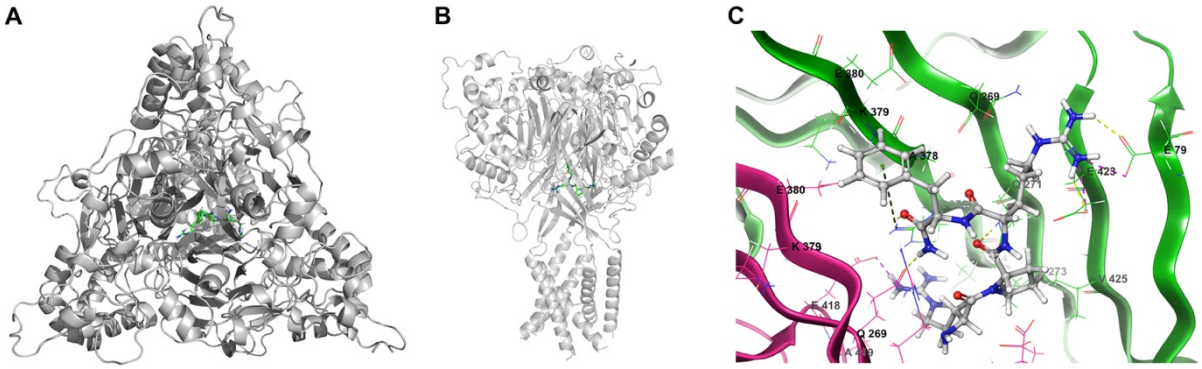

Figure 3

Molecular Pharmacology Fast Forward. Published on July 16, 2018 as DOI: 10.1124/mol.118.112375
This article has not been copyedited and formatted. The final version may differ from this version.

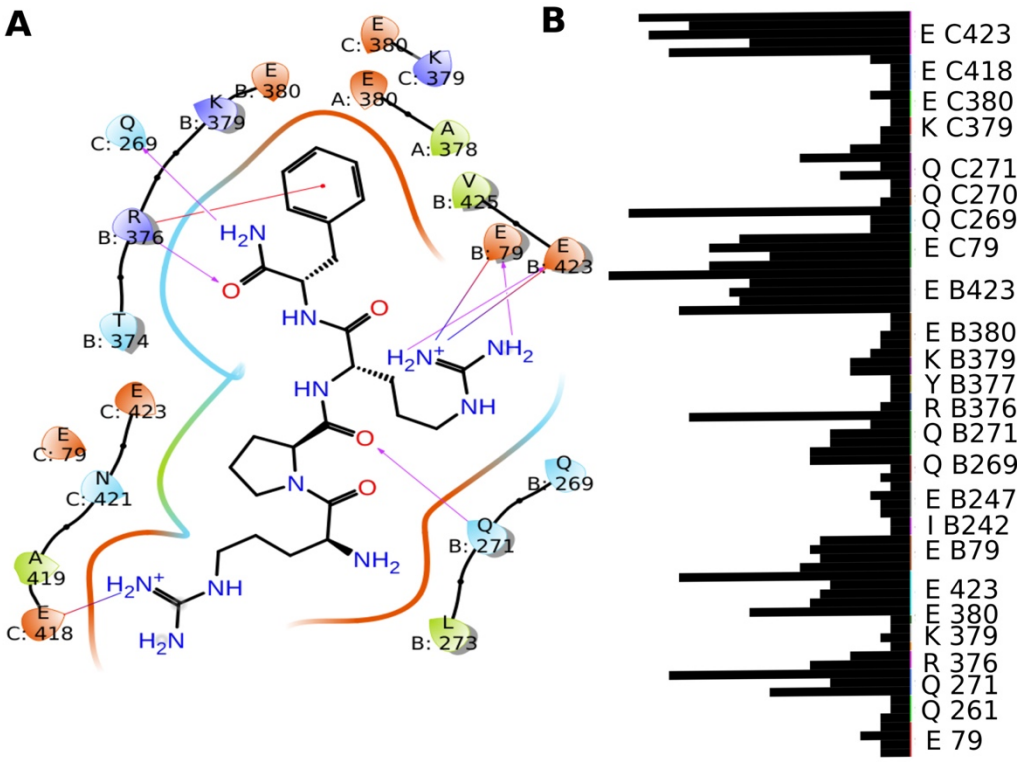

Figure 4

Molecular Pharmacology Fast Forward. Published on July 16, 2018 as DOI: 10.1124/mol.118.112375
This article has not been copyedited and formatted. The final version may differ from this version.

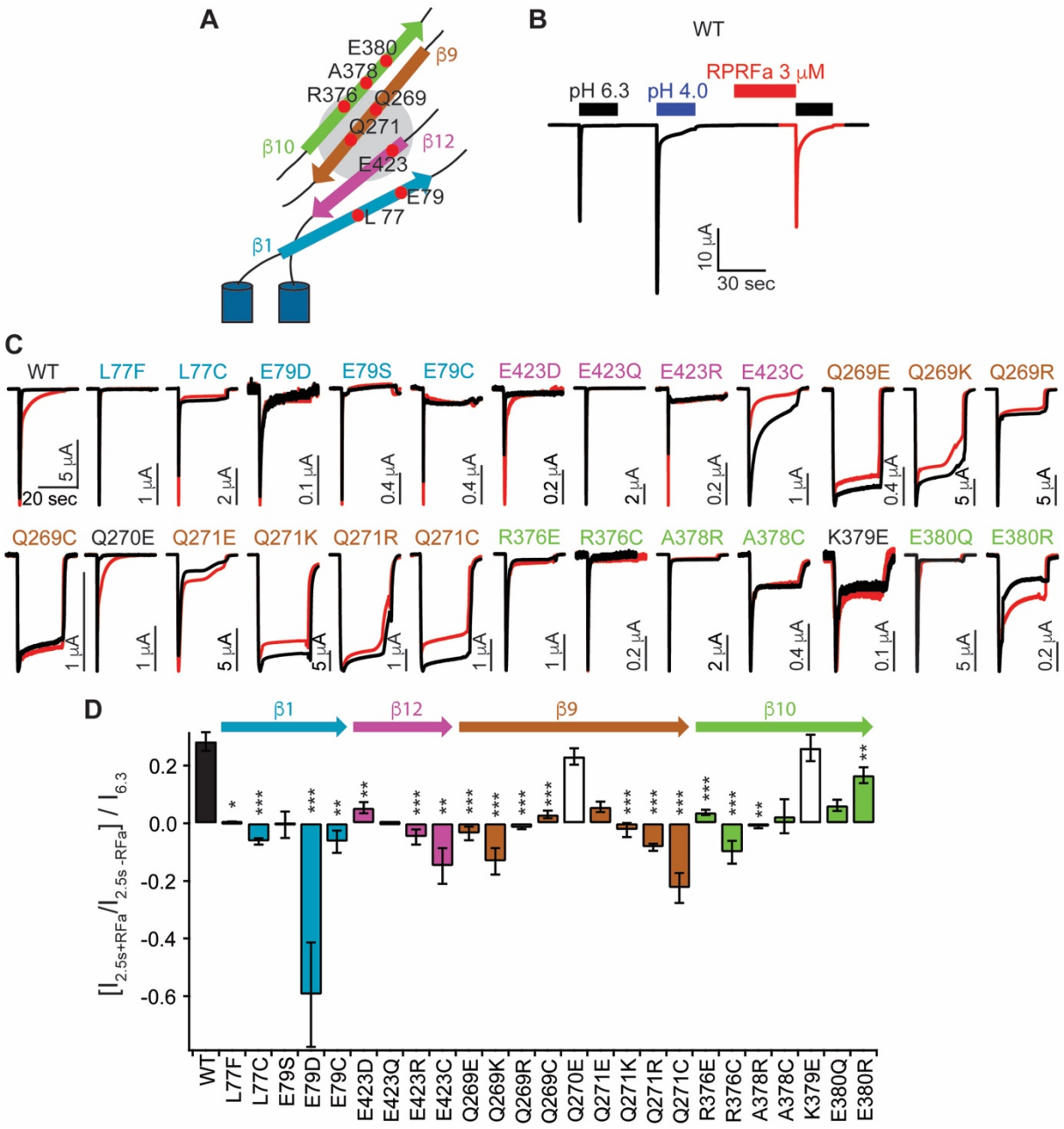

Figure 5

Molecular Pharmacology Fast Forward. Published on July 16, 2018 as DOI: 10.1124/mol.118.112375
This article has not been copyedited and formatted. The final version may differ from this version.

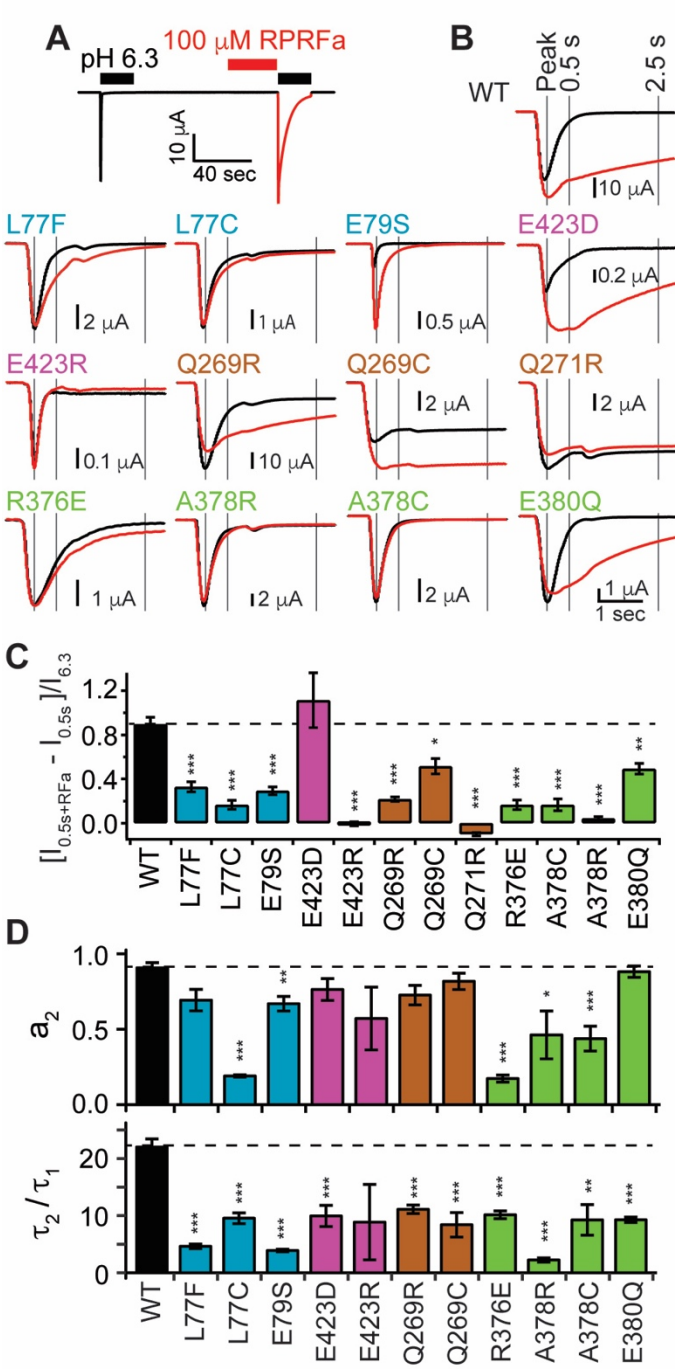

Figure 6

Molecular Pharmacology Fast Forward. Published on July 16, 2018 as DOI: 10.1124/mol.118.112375
This article has not been copyedited and formatted. The final version may differ from this version.

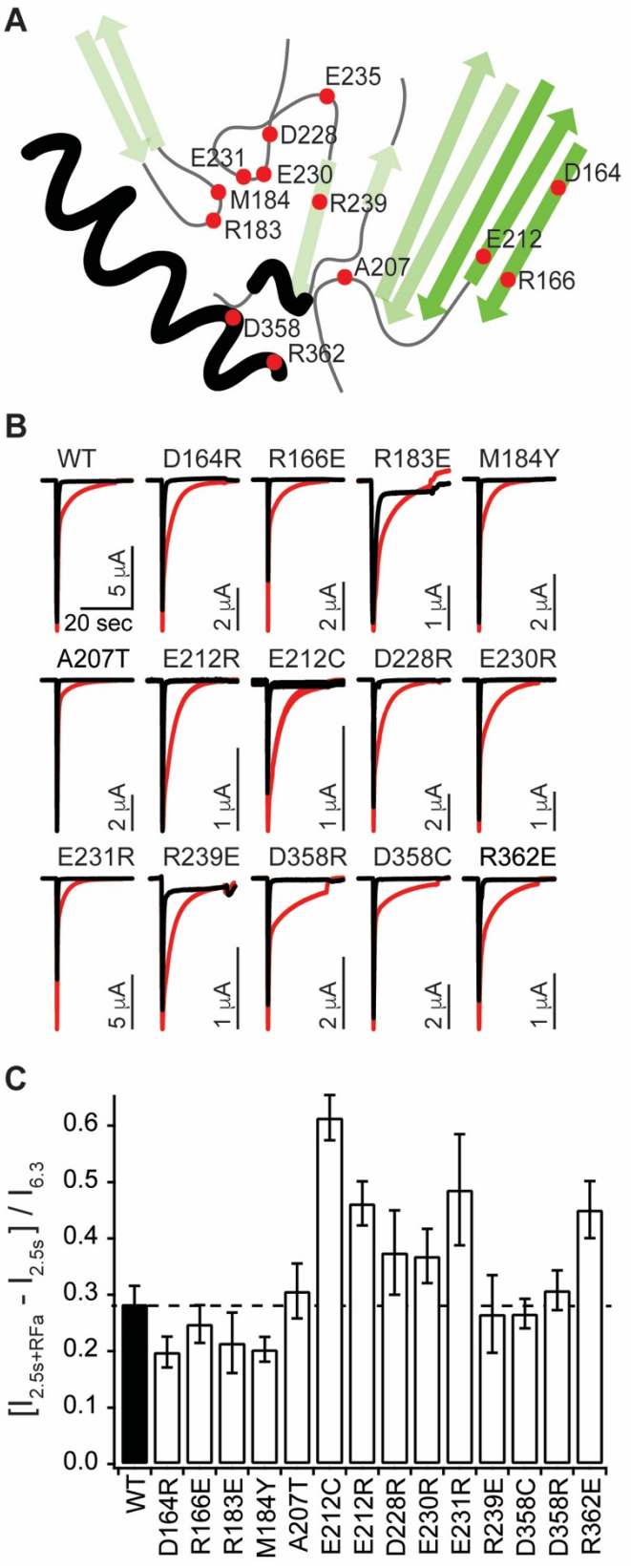

Figure 7

The conoRFamide RPRFa stabilizes the open conformation of Acid-Sensing Ion Channel 3 via the nonproton ligand sensing domain

Melissa Reiners, Michael A. Margreiter, Adrienne Oslender-Bujotzek, Giulia Rossetti, Stefan Gründer, and Axel Schmidt

Molecular Pharmacology

Supporting Information

Supplemental Figure 1. Knowledge-based homology model of rat ASIC3 in the open conformation.

Supplemental Figure 2. Knowledge-based homology model of rat ASIC3 in the desensitized conformation.

Supplemental Figure 3. Knowledge-based homology model of rat ASIC3 in the open conformation in complex with RPRFa in its best-ranked docking pose.

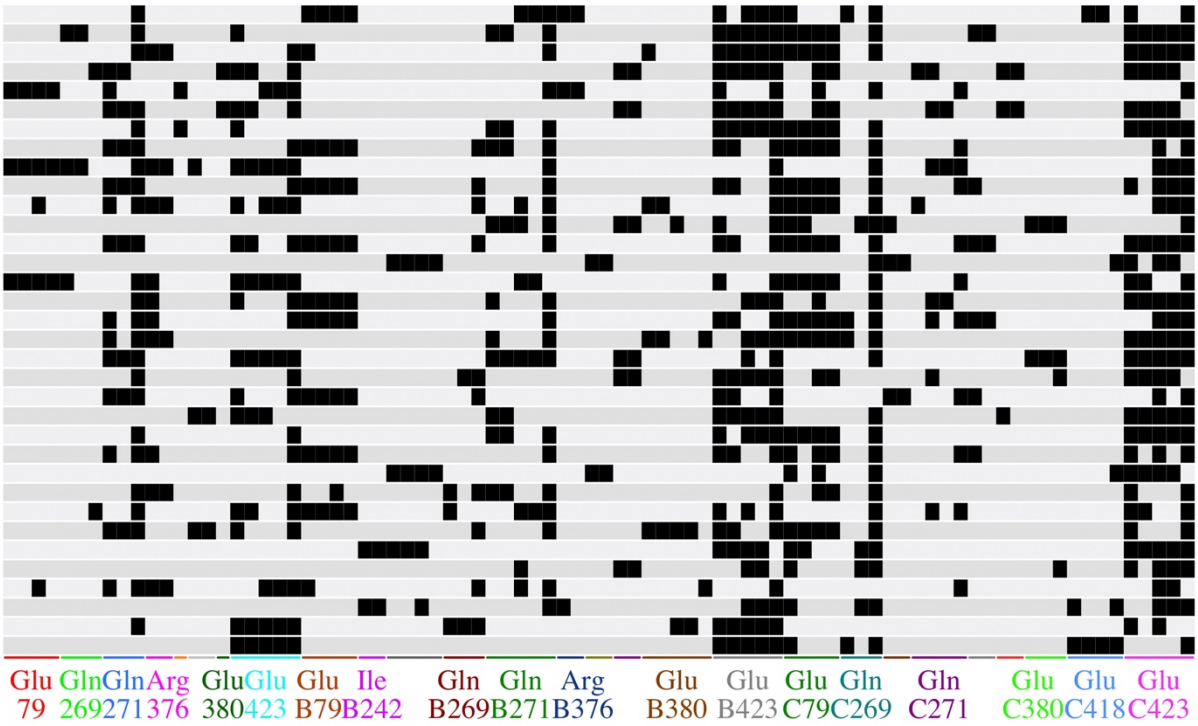

Supplemental Figure 4. Protein-ligand interaction fingerprint (PLIF) shown in Fig. 4 in barcode representation. All receptor amino acids that form at least one protein-peptide interaction are listed. A row represents one particular binding pose and interactions are highlighted as black squares. Better scoring poses are on the top (more negative Emodel scores). Depending on the interacting receptor amino acid, several different interactions (e.g. salt bridges, π-stacking) can be formed. Thus, there are varying numbers of corresponding columns.

Supplemental Figure 5. Movie showing from different perspectives the homology model of ASIC3 in the open conformation in complex with RPRFa in its best-ranked docking pose.

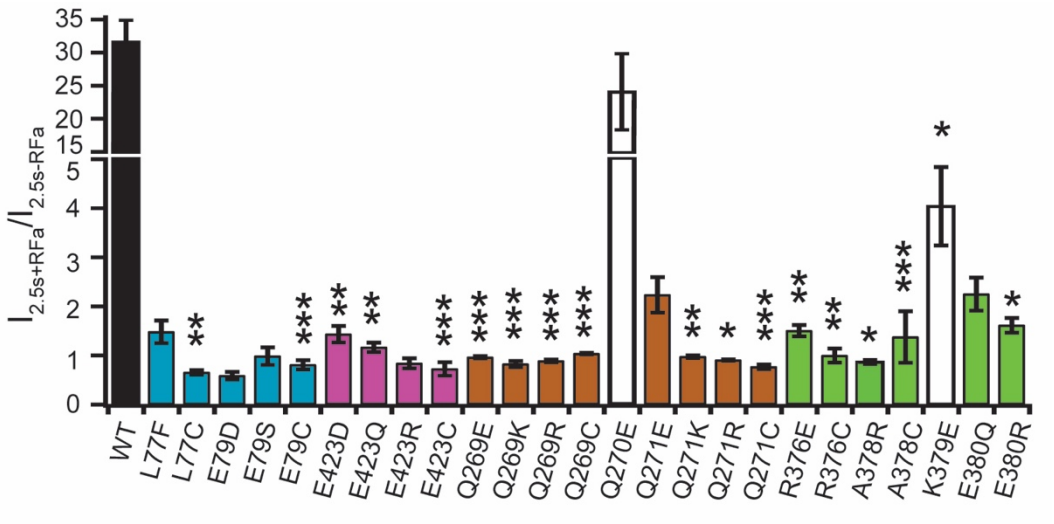

Supplemental Figure 6. Mean $I_{2.5s+RFa}/I_{2.5s}$ ratios for all 25 mutants of the NPLSD. Bar graph showing mean ratios of current amplitudes 2.5 sec post-peak in the absence of and after pre-incubation with RPRFamide ($I_{2.5s+RFa}/I_{2.5s}$). Bars are shown in the colour of the corresponding β strands in Fig. 5A; the white bars represent residues whose side chains point away from the cavity. Note that the y-axis has two different scales. Error bars indicate SEM. n_{mutant} = 8-19; n_{wt} = 4-28 (each condition), n_{wt} (total) = 102. *, $P < 0.05$; **, $P < 0.01$; ***, $P < 0.001$ (Student´s t-test followed by Bonferroni correction).

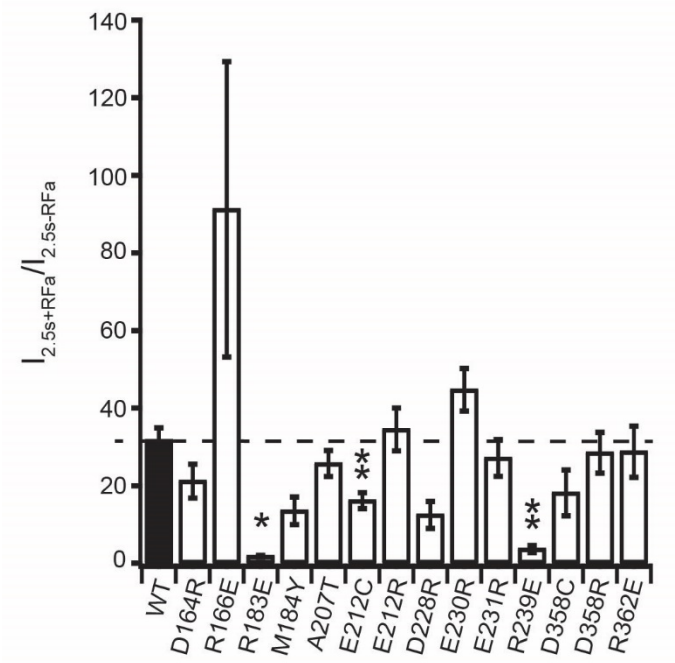

Supplemental Figure 7. Mean $I_{2.5s+RFa}/I_{2.5s}$ ratios for all 12 mutants of the acidic pocket. The dotted line represents the ratio of the wild type as reference. Error bars indicate SEM. n_{mutant} = 8-18; n_{wt} = 6-20 (each condition), n_{wt} (total) = 102. *, $P < 0.05$; **, $P < 0.01$ (Student´s t-test followed by Bonferroni correction).

SiteMap Results		SiteScore	Volume (Å^3)
Open Model	Site #1 (AP)	1.10	820
	Site #2 (NPLSD)	1.06	3484
	Site #3	1.03	884
	Site #4	1.02	919
	Site #5	1.00	968
Desensitized Model	Site #1 (AP1)	1.11	631
	Site #2	1.10	497
	Site #3 (AP2)	1.08	700
	Site #4	1.00	874
	Site #5	0.99	1180

Supplemental Table 1. Potential binding sites on ASIC3. Binding sites were detected with SiteMap (see Methods). SiteScore values and volume of the sites are indicated. Potential binding sites were sorted according to SiteScore for the individual models. The NPLSD is only detected in the open state model. The acidic pocket (AP) is detected twice in the desensitized state model, due to receptor symmetry. In the open state model, the AP is ranked slightly higher than the NPLSD.

RPRFamide Conformer	Docking Score	Glide Emodel Score
1	-7.28	-110.92
2	-8.26	-109.83
3	-8.30	-105.80
4	-5.02	-102.57
5	-6.33	-101.56
6	-5.75	-93.37
7	-6.80	-91.31
8	-5.53	-91.15
9	-5.37	-90.17
10	-5.51	-88.82
11	-6.80	-88.74
12	-5.75	-88.62
13	-5.76	-88.53
14	-4.51	-83.92
15	-5.52	-83.06
16	-5.76	-82.05
17	-5.41	-81.59
18	-5.59	-77.51
19	-6.23	-76.98
20	-6.57	-76.21
21	-4.62	-75.22
22	-4.78	-73.97
23	-6.54	-73.51
24	-4.50	-66.57
25	-3.20	-66.21
26	-4.31	-64.91
27	-5.28	-64.48
28	-5.33	-64.16
29	-5.58	-63.72
30	-3.13	-61.05
31	-4.87	-57.34
32	-4.28	-57.13
33	-4.28	-54.60
34	-6.49	-54.27

Supplemental Table 2. Docking scores of RPRFamide binding poses.

Mutant	$I_{pH6.3}$ (μA)	$[I_{2.5s+RFa} - I_{2.5s-RFa}]/I_{pH6.3}$	$I_{2.5s+RFa}/I_{2.5s-RFa}$	$I_{pH6.3} / I_{pH4.0}$	n
WT	-11.0±1.0	0.28±0.03	31.68±3.27	0.55±0.02	100-102
L77C	-5.3±1.2**	-0.06±0.01***	0.66±0.04**	0.30±0.02***	11
L77F	-6.3±1.3	0±0*	1.50±0.21	0.27±0.03**	11
E79D	-0.1±0*	-0.60±0.18***	0.59±0.08	0.15±0.02***	10
E79S	-0.5±0.2	-0.01±0.05	1.03±0.16	0.12±0.02***	11
E79C	-0.6±0.1***	-0.06±0.04***	0.81±0.09***	0.23±0.02***	17
E423D	-0.3±0.1**	0.05±0.02**	1.43±0.16**	0.22±0.02***	19
E423Q	-7.7±2.4	0±0	1.17±0.10**	0.31±0.06	10
E423R	-0.2±0*	-0.05±0.03***	0.81±0.10	0.10±0.02***	12
E423C	-1.1±0.4***	-0.15±0.06**	0.73±0.14***	0.22±0.07**	8
Q269C	-8.4±1.9**	0.03±0.01***	1.04±0.02***	0.54±0.03*	14
Q269E	-0.9±0.2***	-0.04±0.02***	0.96±0.03***	0.78±0.04	12
Q269K	-19.1±2.8	-0.13±0.05***	0.82±0.06***	0.52±0.03	11
Q269R	-13.8±2.6	-0.02±0***	0.89±0.03***	0.49±0.06	12
Q270E	-1.8±0.4***	0.23±0.03	24.15±5.74	0.30±0.03***	11
Q271E	-3.7±1.0	0.06±0.02	2.24±0.36	0.49±0.07	10
Q271K	-17.6±2.3	-0.02±0.02***	0.97±0.03**	0.82±0.03	11
Q271R	-16.8±2.8***	-0.08±0.01***	0.91±0.01*	0.65±0.05**	17-18
Q271C	-1.4±0.3***	-0.23±0.05***	0.77±0.05***	0.44±0.01***	17-18
R376E	-3.5±0.5	0.04±0.01***	1.50±0.12**	0.58±0.04*	9
R376C	-0.2±0**	-0.1±0.04***	1.00±0.14**	0.45±0.05	14-16
A378R	-8.2±2.1	-0.01±0***	0.87±0.04*	0.47±0.03	14
A378C	-0.8±0.4***	0.02±0.06	1.38±0.53***	0.32±0.04**	11
K379E	-0.2±0**	0.26±0.05	4.04±0.80*	0.15±0.03**	9
E380Q	-15.9±2.5*	0.06±0.02	2.25±0.34	0.39±0.04	11
E380R	-0.3±0.1**	0.17±0.03**	1.61±0.15*	0.08±0.01***	9
D164R	-10.5±1.8	0.2±0.03	21.14±4.41	0.51±0.04	9
R166E	-2.5±0.8**	0.25±0.03	91.22±38.07	0.59±0.05	11-12
R183E	-0.6±0.4	0.21±0.05	1.83±0.21*	0.05±0.02***	8
M184Y	-1.3±0.6	0.2±0.02	13.56±3.59	0.30±0.02***	12
A207T	-24.2±5.3	0.31±0.05	25.69±3.37	0.79±0.06	10
E212R	-6.9±2.4	0.46±0.04	34.49±5.54	0.17±0.04***	9
E212C	-0.6±0.2	0.61±0.04	16.11±2.07**	0.10±0.01**	9
D228R	-2.6±0.9	0.37±0.07	12.45±3.49	0.50±0.04	8
E230R	-3.7±1.3	0.37±0.05	44.70±5.47	0.44±0.06	9
E231R	-3.2±0.7**	0.49±0.10	27.15±4.72	0.19±0.01***	18
R239E	-1.5±0.6**	0.27±0.07	3.70±0.95**	0.22±0.08	10
D358R	-5.6±1.4	0.31±0.04	28.49±5.27	0.53±0.05	11
D358C	-3.9±1.0	0.27±0.03	18.12±5.89	0.57±0.04	9
R362E	-4.9±3.0	0.45±0.05	28.76±6.63	0.22±0.05*	12

Supplemental Table 3. Data obtained in the experiments shown in figures 5 and 7. Values are reported as mean ± S.E.M. *, $P < 0.05$; **, $P < 0.01$; ***, $P < 0.001$ (unpaired t-test between recordings of mutants and wild type of the same week followed by Bonferroni correction).

Mutant	$I_{pH\ 6.3}$ (µA)	$[I_{0.5s+RFa} - I_{0.5s-RFa}]/I_{pH6.3}$	$I_{0.5s+RPRFa}/I_{0.5s-RPRFa}$	a_2	τ_1	τ_2/τ_1	n
WT	-13.6±2.0	0.90±0.07	4.96±0.50	0.91±0.03	0.30±0.01	22.0±1.4	15-17
L77F	-5.6±1.6	0.33±0.05***	2.96±0.24	0.69±0.07	0.29±0.06	4.6±0.4***	10
L77C	-1.6±0.6*	0.17±0.04***	1.41±0.08**	0.19±0.01***	0.43±0.06	9.6±0.9***	6
E79S	-1.7±0.3**	0.29±0.04***	7.25±8.26	0.67±0.05**	0.08±0***	3.9±0.2***	8
E423D	-0.2±0.1***	1.11±0.25	4.93±0.56	0.76±0.07	0.60±0.19	9.9±1.9***	9
E423R	-0.2±0***	-0.01±0.02***	0.98±0.21***	0.57±0.21	0.10±0.01***	8.9±6.6	9
Q269R	-16.2±5.0	0.22±0.02***	1.64±0.05***	0.73±0.06	0.31±0.02	11.1±0.7***	9
Q269C	-4.2±1.0	0.51±0.07*	1.70±0.13**	0.82±0.05	0.95±0.36	8.4±2.1***	7-8
Q271R	-17.7±3.5	-0.10±0.01***	0.89±0.02***				12
R376E	-5.4±1.5	0.17±0.04***	1.35±0.09***	0.17±0.02***	0.53±0.04***	10.1±0.7***	7-8
A378R	-9.0±2.8	0.04±0.02***	1.25±0.07***	0.46±0.16*	0.20±0.02**	2.2±0.4***	7-12
A378C	-4.4±1.9	0.17±0.05***	1.45±0.08**	0.44±0.08***	0.53±0.22	9.3±2.7**	8
E380Q	-2.4±0.7**	0.49±0.05**	3.98±0.26	0.88±0.04	0.24±0.02	9.3±0.5***	9

Supplemental Table 4. Data obtained in the experiments shown in figure 6. Values are reported as mean ± S.E.M. *, $P < 0.05$; **, $P < 0.01$; ***, $P < 0.001$ (unpaired t-test followed by Bonferroni correction). Mutant Q271R could not be fitted by a bi-exponential fit.